Stability Analysis of Gradient-Based Distributed Formation Control with Heterogeneous Sensing Mechanism

The Three Robot Case

Chan, Nelson P. K.; Jayawardhana, Bayu; Garcia de Marina, Hector

DOI
10.1109/TAC.2021.3115881

Publication date
2022

Document Version
Accepted author manuscript

Published in
IEEE Transactions on Automatic Control

This article has been accepted for publication in a future issue of this journal, but has not been fully edited. Content may change prior to final publication. Citation information: DOI 10.1109/TAC.2021.3115881, IEEE Transactions on Automatic Control

Stability Analysis of Gradient-Based Distributed Formation Control with Heterogeneous Sensing Mechanism: the Three Robot Case

Nelson P.K. Chan, Bayu Jayawardhana, and Hector Garcia de Marina

***Abstract*—This paper focuses on the stability analysis of a formation shape displayed by a team of mobile robots that uses heterogeneous sensing mechanism. For the setups consisting of three robots, we show that the use of heterogeneous gradient-based control laws can give rise to undesired invariant sets where a distorted formation shape is possibly moving at a constant velocity. We guarantee local asymptotic stability for the correct and desired formation shape. For the setup with one distance and two bearing robots, we identify the conditions such that an incorrect moving formation is locally attractive.**

I. INTRODUCTION

OVER the years, a rich body of work has been developed on realizing a formation shape by a team of mobile robots. The use and active maintenance of a common type of constraint (distance, bearing, angle, relative position) between two neighboring robots have been the basis for achieving robust formation shape [1], [2], [3], [4], [5]. However, neighboring robots controlling constraints using non-reliable sensors lead to unstable formations [6], [7]. If a sensor failure occurs, then one solution might be to withdraw the non-reliable information and consider a heterogeneous sensing setting for a pair of neighboring robots. For instance, in the case of a partial failure of a LIDAR sensor, which can normally provide relative position information, we may still measure bearing information with non-accurate distance information. In this case, it is possible to define heterogeneous constraints on the same edge that still define the same shape (e.g., one robot controls relative position while the other one controls bearing). However, it remains an open problem whether the application of the local gradient-based control law based on the (heterogeneous) information available to each robot can still maintain the formation. Note that communication between robots to recover full information might not be possible by design. Indeed, the aforementioned works on formation with homogeneous information require only local sensing without information exchange between robots. The answer to this problem can open the way to the design of more robust strategies since distance-based/bearing-based controllers are more robust to non-accurate bearing/distance measurements [8], [9]. For example, instead of just controlling relative positions, the bearing measurement becomes less sensitive when the robots move in a large formation shape, or the robots carrying multiple distance and bearing sensors can control the most relevant constraint depending on the accuracy or reliability of the equipped sensor for a given situation (e.g., far versus near, wide-angle versus small-angle, etc.) Intuitively, the gradient-based control law will steer each robot to the direction that minimizes the local potential function and reaches the desired constraints. However, as different types of potential function may be defined for the same edge due to the heterogeneous sensing mechanisms between the robots, the direction that is taken by each robot may not coincide anymore with the minimization of the combined potential functions.

In this work, we consider the formation stabilization problem in which the desired formation shape is specified by a mixed set of distance and bearing constraints. In [9], the authors divide the edges of formation graph into two sets where one set is associated to the distance constraints while the other one corresponds to the bearing constraints. Consequently, there are nodes that are involved in both types of edges, in which case the robots will be equipped with both types of sensor systems. In contrast to [9], we consider instead two disjoint sets of nodes where one set uses distance information while the other one employs bearing information. Analogous to the previous case, there are edges that are defined by both distance and bearing constraints. The presence of multiple constraints in these edges may lead to some robustness issues when each pair of nodes employs different control laws associated to these different constraints. In this paper, we study the robustness of formation keeping in a heterogeneous network where minimal number of sensor systems for formation keeping are deployed per node. Particularly, each robot within the team has the task of maintaining a subset of either the distance or bearing constraints. For this particular work, we focus on teams consisting of three robots. Using standard gradient-based control laws specific to the constraints each robot has to maintain, we analyze the stability property, particularly, the local asymptotic stability of the desired and incorrect formation shapes. It is of interest to study the applicability of these control laws without modifying their local potential functions to incorporate the different constraints on the edges since it allows us to design distributed control laws that is completely dependent on the available local information to the robot and is independent of the eventual deployment of the robot in the formation.

In Section II, preliminary material and problem formulation are presented. In Sections III and IV, we show that the deployment of heterogeneous gradient-based control laws can result in incorrect formation shapes, possibly moving at a constant velocity. Numerical results and conclusions are given in Sections V and VI, respectively.

The work of N.P.K. Chan & B. Jayawardhana was supported by the Region of Smart Factories (ROSF) project financed by REP-SNN and by the STW Smart Industry 2016 programme. The work of H.G. de Marina is supported by the *Ramon y Cajal* 2020 grant from the Spanish Ministry of Science.

N.P.K. Chan is with Delft University of Technology, 2628CD, Delft, the Netherlands (email: n.p.k.chan@tudelft.nl)

B. Jayawardhana is with Engineering and Technology Institute Groningen, University of Groningen, 9747AG, Groningen, the Netherlands (email: b.jayawardhana@rug.nl)

H.G. de Marina is with the Department of Computer Architecture and Automatic Control at the Faculty of Physics, Universidad Complutense de Madrid, 28040, Madrid, Spain (email: hgarciad@ucm.es)

This article has been accepted for publication in a future issue of this journal, but has not been fully edited. Content may change prior to final publication. Citation information: DOI 10.1109/TAC.2021.3115881, IEEE Transactions on Automatic Control

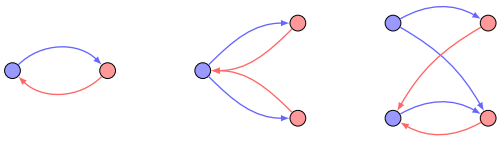

Fig. 1. Examples of complete bipartite digraphs for $n = 2$ and 3 vertices and a bipartite digraph for $n = 4$ vertices. Without loss of generality, ● represents an element of $\mathcal{V}_1$ while ● belongs to $\mathcal{V}_2$. Correspondingly, the blue arrows belong to $\mathcal{V}_1 \times \mathcal{V}_2$ while the red arrows are elements of $\mathcal{V}_2 \times \mathcal{V}_1$.

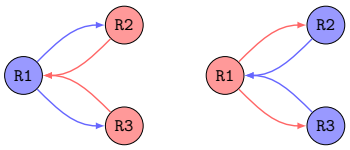

Fig. 2. Setups for the three robot case; ● represents a distance robot and ● represents a bearing robot. Correspondingly, blue arrows are sensing carried out by the distance robots while red arrows represents the edges from the bearing robots. From left to right, we have the (**1D2B**) and (**1B2D**) setup.

II. PRELIMINARIES

A. Graph theory

A *directed graph* (in short, *digraph*) $\mathcal{G}$ is a pair $(\mathcal{V}, \mathcal{E})$, where $\mathcal{V} = \{1, 2, \ldots, n\}$ is the *vertex* set and $\mathcal{E} \subseteq \mathcal{V} \times \mathcal{V}$ is the *edge* set. For $i, j \in \mathcal{V}$, the ordered pair (i, j) represents an edge pointing *from* i *to* j. We assume $\mathcal{G}$ does not have self-loops, i.e., $(i, i) \notin \mathcal{E}$ for all $i \in \mathcal{V}$ and $\mathbf{card}(\mathcal{E}) = m$. The set of neighbors of vertex i is denoted by $\mathcal{N}_i = \{j \in \mathcal{V} \mid (i, j) \in \mathcal{E}\}$. The digraph $\mathcal{G}$ is *bipartite* if the vertex set $\mathcal{V}$ can be partitioned into two subsets $\mathcal{V}_1$ and $\mathcal{V}_2$ with $\mathcal{V}_1 \cap \mathcal{V}_2 = \varnothing$ and the edge set is $\mathcal{E} \subseteq (\mathcal{V}_1 \times \mathcal{V}_2) \cup (\mathcal{V}_2 \times \mathcal{V}_1)$. We assume $\mathbf{card}(\mathcal{V}_1) = n_1$ and hence $\mathbf{card}(\mathcal{V}_2) = n_2 = n - n_1$. For a *complete bipartite digraph*, $\mathcal{E} = (\mathcal{V}_1 \times \mathcal{V}_2) \cup (\mathcal{V}_2 \times \mathcal{V}_1)$ and $\mathbf{card}(\mathcal{E}) = 2n_1n_2$. Fig. 1 depicts complete bipartite digraphs for $n = 2$ and 3 vertices and a bipartite digraph for $n = 4$ vertices.

B. Formations and gradient-based control laws

We consider a team consisting of n robots in which `Ri` is the label assigned to robot i. The robots are moving in the plane according to the single integrator dynamics, i.e.,

$$\dot{p}_i = u_i, \quad i \in \{1, \ldots, n\}, \tag{1}$$

where $p_i \in \mathbb{R}^2$ (a point in the plane) and $u_i \in \mathbb{R}^2$ represent the position of and the control input for `Ri`, respectively. For convenience, all spatial variables are given relative to a global coordinate frame Σ^{g}. The group dynamics is obtained as $\dot{p} = u$ with the stacked vectors $p = \begin{bmatrix} p_1^\top & \cdots & p_n^\top \end{bmatrix}^\top \in \mathbb{R}^{2n}$ representing the team *configuration* and $u = \begin{bmatrix} u_1^\top & \cdots & u_n^\top \end{bmatrix}^\top \in \mathbb{R}^{2n}$ being the collective input. The interactions among the robots are described by a fixed graph $\mathcal{G}(\mathcal{V}, \mathcal{E})$ with $\mathcal{V}$ representing the team of robots and $\mathcal{E}$ containing the neighboring relationships. We embed $\mathcal{G}$ into the plane by assigning to each robot $i \in \mathcal{V}$, a point $p_i \in \mathbb{R}^2$. The pair $\mathcal{F}_p = (\mathcal{G}, p)$ denotes a *framework* (or equivalently a *formation*). We assume $p_i \neq p_j$ if $i \neq j$, i.e., two robots cannot be at the same position. We introduce the following notation prior to providing details on the *distance-based* and *bearing-only* formation control approaches. For points p_i and p_j, we define, relative to Σ^{g}, the relative position as $z_{ij} = p_j - p_i \in \mathbb{R}^2$, the distance as $d_{ij} = \|z_{ij}\| \in \mathbb{R}_{>0}$, and the relative bearing as $g_{ij} = \frac{z_{ij}}{d_{ij}} \in \mathbb{R}^2$. It follows $z_{ji} = -z_{ij}$, $d_{ji} = d_{ij}$ and $g_{ji} = -g_{ij}$.

1) Distance-based formation control: In *distance-based* formation control, a *desired formation* is characterized by a set of *inter-robot distance constraints*. Assume the desired distance between a robot pair (i, j) of the formation is $d_{ij}^\star$ and let $d_{ij}(t)$ be the current distance at time t. Let us define the *distance error* signal as $e_{ij\mathrm{d}}(t) = d_{ij}^2(t) - \left(d_{ij}^\star\right)^2$. A distance-based potential function for (i, j) takes the form $V_{ij\mathrm{d}}(e_{ij\mathrm{d}}) = \frac{1}{4} e_{ij\mathrm{d}}^2$. It has a minimum at the desired distance $d_{ij}^\star$, i.e., $V_{ij\mathrm{d}}(e_{ij\mathrm{d}}) \geqslant 0$ and $V_{ij\mathrm{d}}(e_{ij\mathrm{d}}) = 0 \iff d_{ij} = d_{ij}^\star$. In this case, the corresponding gradient-based control law for maintaining distance $d_{ij}^\star$ for the robot pair (i, j) is $u_{ij\mathrm{d}} = e_{ij\mathrm{d}} z_{ij}$, where z_{ij} is the measurement that `Ri` obtains from its neighbor $j \in \mathcal{N}_i$. Thus the distanced-based formation control law for robot `Ri` in (1) is given by

$$u_{i\mathrm{d}} = \sum_{j \in \mathcal{N}_i} e_{ij\mathrm{d}} z_{ij}. \tag{2}$$

It is well-studied in literature (e.g. [10]) that the above control law guarantees the local exponential stability of the desired formation shape when the desired shape is infinitesimally rigid.

2) Bearing-only formation control: In *bearing-only* formation control, the desired formation is characterized by a set of *inter-robot bearing constraints*. Consider the i-th robot (with label `Ri`) in this setup. Robot `Ri` is able to obtain the bearing measurement $g_{ij}(t)$ from its neighbors $j \in \mathcal{N}_i$ and its goal is to achieve desired bearings $g_{ij}^\star$s with all neighbors $j \in \mathcal{N}_i$. In this case, the *bearing error* signal for a robot pair (i, j) can be defined by $e_{ij\mathrm{b}}(t) = g_{ij}(t) - g_{ij}^\star$. The corresponding potential function is $V_{ij\mathrm{b}}(e_{ij\mathrm{b}}) = \frac{1}{2} d_{ij} \|e_{ij\mathrm{b}}\|^2$. Note that $V_{ij\mathrm{b}}(e_{ij\mathrm{b}}) \geqslant 0$ and it is only zero when $d_{ij} = 0$ or $e_{ij\mathrm{b}} = \mathbb{0}_2 \iff g_{ij} = g_{ij}^\star$. (In forthcoming analysis, we will show that $d_{ij} = 0$, where robots `Ri` and `Rj` are at the same position, is not a viable option.) It can be verified that $u_{ij\mathrm{b}} = e_{ij\mathrm{b}}$ is the gradient-based control law derived from $V_{ij\mathrm{b}}(e_{ij\mathrm{b}})$ for the robot pair (i, j). The bearing-only formation control law for `Ri` in (1) is then given by

$$u_{i\mathrm{b}} = \sum_{j \in \mathcal{N}_i} e_{ij\mathrm{b}}. \tag{3}$$

In [4], it has been shown that the above control law ensures the global asymptotic stability of the desired formation shape provided the formation shape is infinitesimally bearing rigid.

C. Cubic equations

Lemma 1: Consider the reduced cubic equation $y^3 + cy + d = 0$ with coefficients $c < 0$ and $d > 0$. The discriminant is $\Delta := -4c^3 - 27d^2 \geqslant 0$. Then two positive real roots exist with values

$$\begin{aligned} y_{\mathrm{p}_1} &= 2\sqrt[3]{r_v}\cos\left(\tfrac{1}{3}\varphi_v\right) && \in \left[1, \sqrt{3}\right)\sqrt[3]{r_v}, \\ y_{\mathrm{p}_2} &= 2\sqrt[3]{r_v}\cos\left(\tfrac{1}{3}\varphi_v - 120^\circ\right) && \in (0, 1]\sqrt[3]{r_v}, \end{aligned} \tag{4}$$

where $r_v = \sqrt{-(c/3)^3}$ and $\varphi_v = \tan^{-1}\left(-2/d\sqrt{-R}\right) \in (90^\circ, 180^\circ]$. When $\Delta = 0$, the two positive real roots are equal and have value $y_{\mathrm{p}_1} = y_{\mathrm{p}_2} = \sqrt[3]{r_v} = \sqrt[3]{d/2}$.

The proof of Lemma 1 can be found in [11].

D. Problem formulation

As discussed in the Introduction, we study the setup in which the robots possess heterogeneous sensing, and each robot, depending on its own local information, maintains the prescribed distance or bearing with its neighbors using the aforementioned distance-based or bearing-only formation control law. Thus in the current setup, each robot fulfills either a *distance task* or a *bearing task*. As before, consider a pair of robots with labels `Ri` and `Rj`. In case `Ri` is assigned a distance task, its goal is to maintain a desired distance $d^\star_{ij}$ with `Rj`. To attain this goal, it makes use of the distance-based control law $u_{ij\mathrm{d}} = e_{ij\mathrm{d}} z_{ij}$ with z_{ij} being the obtained relative position measurement relative to a local coordinate frame Σ^{i}. Note that Σ^{i} is *not necessarily aligned* with Σ^{j} or Σ^{g}. On the other hand, when `Rj` is assigned a bearing task, its goal is to maintain a desired bearing $g^\star_{ji}$ with `Ri`. It reaches this goal by employing the bearing-only control law $u_{ij\mathrm{b}} = e_{ij\mathrm{b}}$ based on the obtained relative bearing measurement g_{ij} relative to Σ^{j} which is *aligned* with Σ^{g}. For the interconnection topology, we assume each robot has only neighbors of the opposing category, i.e., a distance robot can only have edges with bearing robot(s) and vice versa. As a result, the team of n robots can be partitioned into two sets, namely the set of distance robots $\mathcal{D}$ and the set of bearing robots $\mathcal{B}$ with $\mathcal{D} \neq \varnothing$ and $\mathcal{B} \neq \varnothing$. The edge set is given by $\mathcal{E} \subseteq (\mathcal{D} \times \mathcal{B}) \cup (\mathcal{B} \times \mathcal{D})$; the underlying graph structure is that of a bipartite digraph.

In the current work, we focus on the case in which the team of $n = 3$ robots has a *complete bipartite digraph* topology, i.e., the edge set is $\mathcal{E} = (\mathcal{D} \times \mathcal{B}) \cup (\mathcal{B} \times \mathcal{D})$. We distinguish two feasible robot setups, namely the *one distance and two bearing* (**1D2B**) or the *one bearing and two distance* (**1B2D**) setup; see Fig. 2 for an illustration of these setups. For these setups, we are interested in studying the stability of the formation system employing the distance-based formation control law in (2) for the distance robot(s) and the bearing-only formation control law in (3) for the bearing robot(s). In this case, we do not modify the standard gradient-based control law for the different tasks. Consequently, we analyze whether i). the equilibrium set contains undesired shape and/or group motion; ii). the desired shape is (exponentially) stable; and iii). the undesired shape and/or group motion (if any) is attractive. The first and last questions are motivated by the robustness issues of the distance- and displacement-based controllers as studied in [6], [7], [12], [13] where a disagreement between neighboring robots about desired values or measurements can lead to an undesired group motion and deformation of the formation shape. Since we are considering heterogeneous sensing mechanisms with corresponding heterogeneous potential functions, it is of interest whether such undesired behavior can co-exist. Such knowledge on the effect of heterogeneity in the control law can potentially be useful to design simultaneous formation and motion controller as pursued recently in [14].

III. THE (**1D2B**) ROBOT SETUP

In this section, we consider the case of three robots with the partition $\mathcal{D} = \{1\}$ and $\mathcal{B} = \{2, 3\}$; the (**1D2B**) setup in Fig. 2. Utilizing gradient-based control laws for each distance or bearing task, we obtain the following closed-loop dynamics

$$\begin{bmatrix} \dot{p}_1 \\ \dot{p}_2 \\ \dot{p}_3 \end{bmatrix} = \begin{bmatrix} K_{\mathrm{d}} e_{12\mathrm{d}} z_{12} + K_{\mathrm{d}} e_{13\mathrm{d}} z_{13} \\ K_{\mathrm{b}} e_{21\mathrm{b}} \\ K_{\mathrm{b}} e_{31\mathrm{b}} \end{bmatrix}, \tag{5}$$

where we assume the distance robot `R1` has the control gain $K_{\mathrm{d}} > 0$ and the bearing robots `R2` and `R3` the common control gain $K_{\mathrm{b}} > 0$. It is of interest to note that when physical dimension is taken into account with $[\mathrm{L}]$ as the unit of length and $[\mathrm{T}]$ the unit of time, the control gain K_{d} has dimension $[\mathrm{L}]^{-2}[\mathrm{T}]^{-1}$ while K_{b} is expressed in $[\mathrm{L}][\mathrm{T}]^{-1}$. We define the relative position or link vector $z = \begin{bmatrix} z_{12}^\top & z_{13}^\top \end{bmatrix}^\top \in \mathbb{R}^4$. The link dynamics $\dot{z}$ evaluates to

$$\begin{bmatrix} \dot{z}_{12} \\ \dot{z}_{13} \end{bmatrix} = -\begin{bmatrix} K_{\mathrm{b}} e_{12\mathrm{b}} + K_{\mathrm{d}} e_{12\mathrm{d}} z_{12} + K_{\mathrm{d}} e_{13\mathrm{d}} z_{13} \\ K_{\mathrm{b}} e_{13\mathrm{b}} + K_{\mathrm{d}} e_{12\mathrm{d}} z_{12} + K_{\mathrm{d}} e_{13\mathrm{d}} z_{13} \end{bmatrix}. \tag{6}$$

For a triangle, $z_{12} + z_{23} - z_{13} = \mathbb{0}_2$ holds. Hence the dynamics related to link z_{23} evaluates to $\dot{z}_{23} = -K_{\mathrm{b}}(e_{13\mathrm{b}} - e_{12\mathrm{b}})$.

In the following subsections, we rigorously analyze the closed-loop formation system (5) and link dynamics (6).

A. Equilibrium configurations

*Proposition 1 ((**1D2B**) Equilibrium Configurations):* The equilibrium configurations corresponding to the closed-loop formation system (5) belong to the set

$$\mathcal{S}_p = \left\{ p \in \mathbb{R}^6 \,|\, e = \mathbb{0}_6 \right\}, \tag{7}$$

where $e = \begin{bmatrix} e_{12\mathrm{d}} & e_{13\mathrm{d}} & e_{12\mathrm{b}}^\top & e_{13\mathrm{b}}^\top \end{bmatrix}^\top \in \mathbb{R}^6$.

Proof: Setting the left hand side (LHS) of each equation in (5) to the zero vector, we immediately obtain that the bearing constraints for robots `R2` and `R3` are satisfied since $e_{21\mathrm{b}} = -e_{12\mathrm{b}} = \mathbb{0}_2$ and $e_{31\mathrm{b}} = -e_{13\mathrm{b}} = \mathbb{0}_2$. This implies that $d_{21} = d_{12} \neq 0$ and $d_{31} = d_{13} \neq 0$. It remains to solve for $\dot{p}_1 = \mathbb{0}_2$. With the gathered insights, we obtain $e_{12\mathrm{d}} d_{12} g^\star_{12} = -e_{13\mathrm{d}} d_{13} g^\star_{13}$. Since $g^\star_{12} \neq \pm g^\star_{13}$ (the robots are co-linear when $g_{12} = \pm g_{13}$), the expression is satisfied when $e_{12\mathrm{d}} d_{12} = 0$ and $e_{13\mathrm{d}} d_{13} = 0$. Because $d_{12} \neq 0$ and also $d_{13} \neq 0$, we require $e_{12\mathrm{d}} = 0$ and $e_{13\mathrm{d}} = 0$ to hold. ■

B. Moving configurations

During the analysis of the (**1D1B**) setup (see [11] for details), we observed that robots may move with a common velocity w while the predefined constraints are not met. For the (**1D2B**) setup, we explore whether conditions exist such that the formation may move with a common velocity w.

*Proposition 2 ((**1D2B**) Moving Configurations):* The closed-loop formation system (5) moves with a constant velocity $w = K_{\mathrm{b}} b^\star_{\mathrm{sum}}$ with $b_{\mathrm{sum}} = g_{12} + g_{13}$ when the error vector e satisfies

$$e = -\begin{bmatrix} 1/d_{12} R_{\mathrm{bd}} & 1/d_{13} R_{\mathrm{bd}} & b^{\star\top}_{\mathrm{sum}} & b^{\star\top}_{\mathrm{sum}} \end{bmatrix}^\top. \tag{8}$$

Proof: First, we solve for $\dot{z} = \mathbb{0}_4$. Since $\dot{z}_{12} = \mathbb{0}_2 = \dot{z}_{13}$, it follows $\dot{z}_{23} = \mathbb{0}_2$. This expression evaluates to $g_{12} - g_{13} =$

$g_{12}^\star - g_{13}^\star$. Define $b_{\text{diff}} = g_{12} - g_{13}$ and let $\angle g_{12} = \alpha$ be the angle enclosed by vector g_{12} and the positive x-axis of Σ^{g}. Similarly, let $\angle g_{13} = \beta$. We can rewrite b_{diff} as

$$= 2\cos\left(1/2\ (\alpha - \beta_\pi)\right) \begin{bmatrix} \cos\left(1/2\ (\alpha + \beta_\pi)\right) \\ \sin\left(1/2\ (\alpha + \beta_\pi)\right) \end{bmatrix}, \tag{9}$$

where $\beta_\pi = \beta + \pi \pmod{2\pi}$. The expression $\dot{z}_{23} = \mathbb{0}_2$ can be transformed to the following set of angle constraints, namely

$$\begin{cases} \alpha + \beta_\pi = \alpha^\star + \beta_\pi^\star \\ \alpha - \beta_\pi = \alpha^\star - \beta_\pi^\star \end{cases} \iff \begin{cases} \alpha = \alpha^\star \\ \beta = \beta^\star \end{cases} \text{and} \quad \begin{cases} \alpha + \beta_\pi = \alpha^\star + \beta_\pi^\star \\ -(\alpha - \beta_\pi) = \alpha^\star - \beta_\pi^\star \end{cases} \iff \begin{cases} \alpha = \beta^\star + \pi \\ \beta = \alpha^\star - \pi \end{cases}$$
(10) (11)

From (10), we obtain $(g_{12},\, g_{13}) = (g_{12}^\star,\, g_{13}^\star)$ corresponding to the equilibrium configurations in $\mathcal{S}_p$ while the solution in (11) corresponds to $(g_{12},\, g_{13}) = (-g_{13}^\star,\, -g_{12}^\star)$. Subsequently, we obtain $e_{12\text{b}} = e_{13\text{b}} = -\left(g_{12}^\star + g_{13}^\star\right) =: b_{\text{sum}}^\star$; it is sufficient to consider one of the equations in (6). This leads to $\left(-K_{\text{d}} e_{13\text{d}} d_{13}\right) g_{12}^\star + \left(-K_{\text{d}} e_{12\text{d}} d_{12}\right) g_{13}^\star = K_{\text{b}} g_{12}^\star + K_{\text{b}} g_{13}^\star$. For it to hold, we require $-K_{\text{d}} e_{13\text{d}} d_{13} = K_{\text{b}} \iff e_{13\text{d}} = -1/d_{13} R_{\text{bd}}$ and $-K_{\text{d}} e_{12\text{d}} d_{12} = K_{\text{b}} \iff e_{12\text{d}} = -1/d_{12} R_{\text{bd}}$ with the gain ratio $R_{\text{bd}} = \frac{K_{\text{b}}}{K_{\text{d}}}$. Collecting the error constraints, we obtain (8). By an immediate substitution, we obtain for the dynamics of the bearing robot R2, $\dot{p}_2 = K_{\text{b}} b_{\text{sum}}^\star =: w$. ∎

Remark 1: The signed area for a triangle can be obtained using the expression $S_{\text{A}} = z_{12}^\top \left[\begin{smallmatrix} 0 & 1 \\ -1 & 0 \end{smallmatrix}\right] z_{13}$ [15], [16]. The signed area of the desired formation shape evaluates to $S_{\text{A}}^\star = d_{12}^\star d_{13}^\star g_{12}^{\top\star} \left[\begin{smallmatrix} 0 & 1 \\ -1 & 0 \end{smallmatrix}\right] g_{13}^\star$. The signed area of the moving formation shape is $S_{\text{A}_\text{M}} = d_{12} d_{13} g_{13}^{\top\star} \left[\begin{smallmatrix} 0 & 1 \\ -1 & 0 \end{smallmatrix}\right] g_{12}^\star = -d_{12} d_{13} g_{12}^{\top\star} \left[\begin{smallmatrix} 0 & 1 \\ -1 & 0 \end{smallmatrix}\right] g_{13}^\star = -\frac{d_{12} d_{13}}{d_{12}^\star d_{13}^\star} S_{\text{A}}^\star$. Since the distance error signals in (8) are negative, it follows $d_{ij} < d_{ij}^\star$. Hence $|S_{\text{A}_\text{M}}| < |S_{\text{A}}|$ and the cyclic ordering of the robots is opposite to that of the desired formation shape.

Following Proposition 2, a characterization of the moving set $\mathcal{T}_p$ in terms of the error vector e is

$$\mathcal{T}_p = \left\{ p \in \mathbb{R}^6 \,|\, e \text{ satisfies (8)} \right\}. \tag{12}$$

An equivalent characterization of $\mathcal{T}_p$ can be provided in terms of the inter-robot relative position vectors z_{12_M} and z_{13_M} where subscript $_\text{M}$ refers to "moving". In fact, the inter-robot bearing vectors g_{12_M} between R1 and R2 and g_{13_M} between robots R1 and R3 is known from the proof of Proposition 2. It remains to obtain feasible values for the inter-robot distances d_{12_M} and d_{13_M}. To this end, we find the roots satisfying the expressions for the distance error signals $e_{12\text{d}}$ and $e_{13\text{d}}$ in (8). Expanding the expressions leads to the following cubic equation

$$d_{ij}^3 - \left(d_{ij}^\star\right)^2 d_{ij} + R_{\text{bd}} = 0, \quad ij \in \{12,\, 13\}. \tag{13}$$

Compared with Lemma 1, we have $c = -\left(d_{ij}^\star\right)^2 < 0$ and $d = R_{\text{bd}} > 0$. We obtain the discriminant corresponding to (13) is $\Delta = 4\left(d_{ij}^\star\right)^6 - 27 R_{\text{bd}}^2$ and the threshold value for the desired distance $d_{ij}^\star$ such that positive roots exist is $\widehat{d} = \sqrt{3}\sqrt[3]{R_{\text{bd}}/2} \approx 1.3747 \sqrt[3]{R_{\text{bd}}}$. We infer that if one of (or both) the desired distances $d_{12}^\star$ or (and) $d_{13}^\star$ has (have) a value less than $\widehat{d}$, then no feasible value for d_{12} or (and) d_{13} satisfies $e_{12\text{d}} d_{12} = -R_{\text{bd}}$ or (and) $e_{13\text{d}} d_{13} = -R_{\text{bd}}$, implying the in-feasibility of moving formations. We conclude the set $\mathcal{S}_p$ containing equilibrium configurations with one of (or both) $d_{12}^\star < \widehat{d}$ or (and) $d_{13}^\star < \widehat{d}$ is globally asymptotically stable.

When the desired distances $d_{ij}^\star$s satisfy $d_{ij}^\star \geqslant \widehat{d}$, we obtain feasible distances d_{ij} to (13) are given by Lemma 1 with the values $r_v = \sqrt{\left(d_{ij}^\star\right)^6/27}$ and $\varphi_v = \tan^{-1}\left(-2R_{\text{bd}}^{-1}\sqrt{-R}\right)$. Since we have two desired distances $d_{12}^\star$ and $d_{13}^\star$ and we have either one or two feasible value(s) d_{ij} to the cubic equation (13), it follows that different feasible combinations $(d_{12_\text{M}},\, d_{13_\text{M}})$ exist. We have the following cases:

- $(d_{12}^\star,\, d_{13}^\star) = \left(\widehat{d},\, \widehat{d}\right)$; 1 combination for $(d_{12_\text{M}},\, d_{13_\text{M}})$;
- $(d_{12}^\star,\, d_{13}^\star) = \left(\widehat{d},\, > \widehat{d}\right)$; 2 combinations for $(d_{12_\text{M}},\, d_{13_\text{M}})$;
- $(d_{12}^\star,\, d_{13}^\star) = \left(> \widehat{d},\, \widehat{d}\right)$; 2 combinations for $(d_{12_\text{M}},\, d_{13_\text{M}})$;
- $(d_{12}^\star,\, d_{13}^\star) > \left(\widehat{d},\, \widehat{d}\right)$; 4 combinations for $(d_{12_\text{M}},\, d_{13_\text{M}})$;

We conclude the set $\mathcal{T}_p$ is a non-empty set when the additional constraints $d_{12}^\star \geqslant \widehat{d}$ and $d_{13}^\star \geqslant \widehat{d}$ are satisfied.

Recall the common velocity $w = K_{\text{b}} b_{\text{sum}}$ for the robots in Proposition 2. We want to write b_{sum} in the form $b_{\text{sum}} = d_{\text{sum}}\, g_{\text{sum}}$ with d_{sum} being the magnitude and g_{sum} the orientation of b_{sum} relative to Σ^{g}. By the sum-to-product identities for cosine and sine, we obtain

$$b_{\text{sum}} = 2\cos\left(1/2\ (\alpha - \beta)\right) \begin{bmatrix} \cos\left(1/2\ (\alpha + \beta)\right) \\ \sin\left(1/2\ (\alpha + \beta)\right) \end{bmatrix}. \tag{14}$$

Depending on the value of the angle difference $|\alpha - \beta|$, we have different expressions for d_{sum} and g_{sum}. When $|\alpha - \beta| < \pi$, we set $d_{\text{sum}} = 2\cos\left(1/2\,|\alpha - \beta|\right)$ and $\angle g_{\text{sum}} = 1/2\ (\alpha + \beta)$ while for $|\alpha - \beta| > \pi$, we set $d_{\text{sum}} = 2\cos\left(\pi - 1/2\,|\alpha - \beta|\right)$ and $\angle g_{\text{sum}} = 1/2\ (\alpha + \beta) + \pi \pmod{2\pi}$. Note that $d_{\text{sum}} \in (0,\, 2)$ for $|\alpha - \beta| \gtrless \pi$. If $|\alpha - \beta| = 0°$, then $g_{12} = g_{13}$ and $b_{\text{sum}} = 2g_{12}$, and finally, $|\alpha - \beta| = \pi$ implies $g_{12} = -g_{13}$ and $b_{\text{sum}} = \mathbb{0}_2$. Since $g_{12}^\star \neq \pm g_{13}^\star$, the last two mentioned cases does not occur; therefore, the magnitude of w is $0 < \|w\| < 2K_{\text{b}}$.

C. Local stability analysis of the equilibrium and moving formations

Assume the desired distances satisfy $d_{12}^\star \geqslant \widehat{d}$ and $d_{13}^\star \geqslant \widehat{d}$. In this case, both the equilibrium configurations in (7) and moving configurations in (12) satisfy $\dot{z} = \mathbb{0}_4$ and are feasible. We are interested in determining the local stability around these formations. To this end, we consider the linearization of the z-dynamics (6); this results in the Jacobian matrix $A \in \mathbb{R}^{4\times 4}$ as

$$A = -\begin{bmatrix} K_{\text{b}} A_{12\text{b}} + K_{\text{d}} A_{12\text{d}} & K_{\text{d}} A_{13\text{d}} \\ K_{\text{d}} A_{12\text{d}} & K_{\text{b}} A_{13\text{b}} + K_{\text{d}} A_{13\text{d}} \end{bmatrix}, \tag{15}$$

where $A_{ij\text{d}} = e_{ij\text{d}} I_2 + 2 z_{ij} z_{ij}^\top$ and $A_{ij\text{b}} = \frac{1}{d_{ij}} P_{g_{ij}}$, with $P_{g_{ij}} = I_2 - g_{ij} g_{ij}^\top$ and $ij \in \{12,\, 13\}$.

We first consider the stability analysis around the equilibrium configurations.

Theorem 1: Consider a team of three robots arranged in the (**1D2B**) setup with closed-loop dynamics given by (5). Assume the desired distances satisfy $d_{12}^\star \geqslant \widehat{d}$ and $d_{13}^\star \geqslant \widehat{d}$ with $\widehat{d} = \sqrt{3}\sqrt[3]{R_{\text{bd}}/2}$ and the bearing vectors satisfy $g_{12}^\star \neq \pm g_{13}^\star$. Given an initial configuration $p(0)$ that is close to the desired formation shape, then the robot trajectories asymptotically converge to a point $\widehat{p} \in \mathcal{S}_p$.

Proof:

This article has been accepted for publication in a future issue of this journal, but has not been fully edited. Content may change prior to final publication. Citation information: DOI 10.1109/TAC.2021.3115881, IEEE Transactions on Automatic Control

Evaluating the Jacobian matrix (15) at the equilibrium configurations results in

$$A_{\mathrm{E}} = -\begin{bmatrix} x^\star & 0 \\ 0 & p^\star \end{bmatrix} \otimes I_2 - \begin{bmatrix} m^\star g_{12}^\star g_{12}^{\star\top} & q^\star g_{13}^\star g_{13}^{\star\top} \\ y^\star g_{12}^\star g_{12}^{\star\top} & n^\star g_{13}^\star g_{13}^{\star\top} \end{bmatrix}, \tag{16}$$

where we define the variables

$$\begin{aligned} x &= K_{\mathrm{b}} d_{12}^{-1}, \quad y = 2K_{\mathrm{d}} d_{12}^2, \quad m = y - x, \\ p &= K_{\mathrm{b}} d_{13}^{-1}, \quad q = 2K_{\mathrm{d}} d_{13}^2, \quad n = q - p, \end{aligned} \tag{17}$$

and the matrices

$$g_{12}^\star g_{12}^{\star\top} = \begin{bmatrix} a^2 & ab \\ ab & b^2 \end{bmatrix}, \quad g_{13}^\star g_{13}^{\star\top} = \begin{bmatrix} c^2 & cd \\ cd & d^2 \end{bmatrix}. \tag{18}$$

The starred version for x, p, y, q, m, and n is used here since we have $d_{12} = d_{12}^\star$ and $d_{13} = d_{13}^\star$. The characteristic polynomial $\chi_{\mathrm{E}}(\lambda)$ corresponding to matrix A_{E} is obtained as

$$\begin{aligned} \chi_{\mathrm{E}}(\lambda) = (\lambda + x^\star)(\lambda + p^\star)\ldots \\ \left(\lambda^2 + (y^\star + q^\star)\lambda + y^\star q^\star \sin^2\theta^\star\right), \end{aligned} \tag{19}$$

where $\sin\theta = g_{12}^\top \left[\begin{smallmatrix} 0 & 1 \\ -1 & 0 \end{smallmatrix}\right] g_{13}$. The roots of (19) are

$$\begin{aligned} &\lambda_1 = -x^\star, \quad \lambda_2 = -p^\star, \\ &\lambda_{3,4} = -1/2\,(y^\star + q^\star) \pm 1/2\sqrt{(y^\star + q^\star)^2 - 4y^\star q^\star \sin^2\theta^\star}. \end{aligned} \tag{20}$$

It can be verified that $0 < 4y^\star q^\star \sin^2\theta^\star \leqslant (y^\star + q^\star)^2$; all roots are real. Moreover, $-(y^\star + q^\star) + \sqrt{(y^\star + q^\star)^2 - 4y^\star q^\star \sin^2\theta^\star} < 0$ and we conclude all λs are negative; matrix A_{E} is Hurwitz. This implies the link trajectories asymptotically converge to the desired relative positions $z^\star$ as $t \to \infty$. It also means the robots accomplish their individual tasks since $z_{ij}^\star = d_{ij}^\star g_{ij}^\star$, so $p(t) \to \mathcal{S}_p$ when $p(0)$ is close to the desired formation shape. ∎

We continue with determining the stability of the moving formations in the set $\mathcal{T}_p$. Based on the characterization in (8), we obtain the Jacobian matrix

$$A_{\mathrm{M}} = -\begin{bmatrix} 0 & p \\ x & 0 \end{bmatrix} \otimes I_2 - \begin{bmatrix} m g_{13}^\star g_{13}^{\star\top} & q g_{12}^\star g_{12}^{\star\top} \\ y g_{13}^\star g_{13}^{\star\top} & n g_{12}^\star g_{12}^{\star\top} \end{bmatrix}, \tag{21}$$

where the variables are defined as in (17) and (18). The corresponding characteristic polynomial $\chi_{\mathrm{M}}(\lambda)$ is the quartic polynomial

$$\chi_{\mathrm{M}}(\lambda) = \lambda^4 + c_1\lambda^3 + c_2\lambda^2 + c_3\lambda + c_4 \tag{22}$$

with the coefficients

$$\begin{aligned} &c_1 = m + n, \quad c_2 = qy\sin^2\theta^\star - px, \quad c_4 = pxmn\sin^2\theta^\star, \\ &c_3 = xm\left(q\sin^2\theta^\star - p\right) + pn\left(y\sin^2\theta^\star - x\right). \end{aligned} \tag{23}$$

Recall that depending on the value of $d_{12}^\star$ and $d_{13}^\star$, we can obtain more than one feasible combination $(d_{12_{\mathrm{M}}}, d_{13_{\mathrm{M}}})$ for the moving configurations. Under certain conditions, we have the following result on the eigenvalues of the matrix A_{M}.

Lemma 2: Assume the desired distances satisfy $d_{12}^\star > \widehat{d}$ and $d_{13}^\star > \widehat{d}$ and the desired bearing vectors are not perpendicular, i.e. $g_{12}^\star \not\perp g_{13}^\star$. Consider the combination $(d_{12_{\mathrm{M}}}, d_{13_{\mathrm{M}}}) = (y_{p_1}(d_{12}^\star), y_{p_1}(d_{13}^\star))$ with y_{p_1} given in Lemma 1. Then all eigenvalues of the matrix A_{M} have a negative real part if the following inequality holds:

$$\cos^2\theta^\star < \frac{mn\left((mq - ny)^2 + mn(m+n)(x+p)\right)}{(m^2q + n^2y)(mqx + nyp)}. \tag{24}$$

Proof: Assuming the bearing vectors are not perpendicular, we obtain that $0 < \sin^2\theta^\star < 1$. Also, since $d_{12_{\mathrm{M}}} = y_{p_1}(d_{12}^\star)$ and $d_{13_{\mathrm{M}}} = y_{p_1}(d_{13}^\star)$ and $d_{12}^\star > \widehat{d}$ and $d_{13}^\star > \widehat{d}$, we verify that $m > 0$ and $n > 0$. We employ the Routh-Hurwitz stability criterion. The first column of the Routh-Hurwitz table, which is the column of interest, contains the following values

$$\left[1 \quad c_1 \quad \frac{c_1c_2 - c_3}{c_1} \quad \frac{(c_1c_2 - c_3)c_3 - c_1^2c_4}{(c_1c_2 - c_3)} \quad c_4\right]. \tag{25}$$

For all roots λ to have negative real parts, all values in (25) need to be positive. With $m > 0$ and $n > 0$, the coefficients c_1 and c_4 are positive. It remains to show the third and fourth entry in (25) is positive. In fact, it is sufficient to show the numerators are both positive. They evaluate to

$$\begin{aligned} &c_1c_2 - c_3 = \sin^2\theta^\star\left(m^2q + n^2y\right) > 0 \\ &(c_1c_2 - c_3)c_3 - c_1^2c_4 = \\ &\quad \sin^2\theta^\star\Big(\left((mq - ny)^2 + mn(m+n)(x+p)\right)mn \\ &\quad - \left(m^2q + n^2y\right)(mxq + npy)\cos^2\theta^\star\Big). \end{aligned} \tag{26}$$

Provided (24) holds, it follows $(c_1c_2 - c_3)c_3 - c_1^2c_4 > 0$. Since the entries in (25) are all positive, we conclude all eigenvalues of the matrix A_{M} have negative real parts. ∎

Remark 2: The implication of Lemma 2 is that under certain conditions on the distance and bearing constraints, a subset of the moving set $\mathcal{T}_p$ is locally asymptotically stable. Hence initializing the robots close to the conditions for the moving formation is not desirable. An illustration of this behavior is provided in Fig. 4(b).

Lemma 2 also holds when the desired bearing vectors are perpendicular, i.e. $g_{12}^\star \perp g_{13}^\star \iff \sin^2\theta^\star = 1$. In this case, the coefficients in (23) and also all entries in (25) are positive; therefore, the matrix A_{M} will only have eigenvalues with negative real parts.

A full characterization of the remaining cases can be found in [11]. In almost all cases, the matrix A_{M} is not Hurwitz.

IV. THE (**1B2D**) ROBOT SETUP

In this section, the formation setup with one bearing and two distance robots (**1B2D**) is considered. Without loss of generality, we assume robot `R1` is the bearing robot while robots `R2` and `R3` are distance robots. The right graph in Fig. 2 depicts the interconnection structure from which the closed-loop dynamics is obtained as

$$\begin{bmatrix} \dot{p}_1 \\ \dot{p}_2 \\ \dot{p}_3 \end{bmatrix} = \begin{bmatrix} K_{\mathrm{b}}e_{12\mathrm{b}} + K_{\mathrm{b}}e_{13\mathrm{b}} \\ K_{\mathrm{d}}e_{21\mathrm{d}}z_{21} \\ K_{\mathrm{d}}e_{31\mathrm{d}}z_{31} \end{bmatrix}. \tag{27}$$

The corresponding link dynamics evaluates to

$$\begin{bmatrix} \dot{z}_{12} \\ \dot{z}_{13} \end{bmatrix} = -\begin{bmatrix} K_{\mathrm{d}}e_{12\mathrm{d}}z_{12} + K_{\mathrm{b}}e_{12\mathrm{b}} + K_{\mathrm{b}}e_{13\mathrm{b}} \\ K_{\mathrm{d}}e_{13\mathrm{d}}z_{13} + K_{\mathrm{b}}e_{12\mathrm{b}} + K_{\mathrm{b}}e_{13\mathrm{b}} \end{bmatrix}. \tag{28}$$

Furthermore, the dynamics of the link z_{23} is found to be $\dot{z}_{23} = -K_{\mathrm{d}}(e_{13\mathrm{d}}z_{13} - e_{12\mathrm{d}}z_{12})$. In the following, we follow similar steps as in Section III for analyzing (27) and (28), focusing on equilibrium configurations, possible moving formations, and their (local) stability analysis.

This article has been accepted for publication in a future issue of this journal, but has not been fully edited. Content may change prior to final publication. Citation information: DOI 10.1109/TAC.2021.3115881, IEEE Transactions on Automatic Control

A. Equilibrium configurations

Proposition 3 ((**1B2D**) *Equilibrium Configurations:):* The equilibrium configurations corresponding to the closed-loop formation system (27) belong to $\mathcal{S}_p^{\mathrm{C}} \cup \mathcal{S}_p^{\mathrm{F}}$, where

$$\begin{aligned}\mathcal{S}_p^{\mathrm{C}} &= \left\{p \in \mathbb{R}^6 \,|\, e = \mathbb{0}_6\right\} \text{ and} \\ \mathcal{S}_p^{\mathrm{F}} &= \left\{p \in \mathbb{R}^6 \,|\, e = \begin{bmatrix} 0 & 0 & -b_{\mathrm{diff}}^{\star\top} & b_{\mathrm{diff}}^{\star\top}\end{bmatrix}^\top\right\},\end{aligned} \tag{29}$$

with $e = \begin{bmatrix} e_{12\mathrm{d}} & e_{13\mathrm{d}} & e_{12\mathrm{b}}^\top & e_{13\mathrm{b}}^\top\end{bmatrix}^\top \in \mathbb{R}^6$ and $b_{\mathrm{diff}}^\star = g_{12}^\star - g_{13}^\star$.

Proof: Setting the LHS of each equation of (27) to the zero vector, we obtain for robot R2 that $-K_{\mathrm{d}} e_{12\mathrm{d}} z_{12} = \mathbb{0}_2 \iff e_{12\mathrm{d}} = 0 \vee z_{12} = \mathbb{0}_2$ and similarly, we have $-K_{\mathrm{d}} e_{13\mathrm{d}} z_{13} = \mathbb{0}_2 \iff e_{13\mathrm{d}} = 0 \vee z_{13} = \mathbb{0}_2$ for R3. The expression for R1 evaluates to $g_{12} + g_{13} = g_{12}^\star + g_{13}^\star$. Defining $\angle g_{12} = \alpha$, $\angle g_{13} = \beta$ as before, and recalling the RHS of (14), we can write the following set of angle constraints, namely

$$\begin{cases}\alpha+\beta=\alpha^\star+\beta^\star \\ \alpha-\beta=\alpha^\star-\beta^\star\end{cases} \iff \begin{cases}\alpha=\alpha^\star \\ \beta=\beta^\star\end{cases} \text{ and } \tag{30}$$

$$\begin{cases}\alpha+\beta=\alpha^\star+\beta^\star \\ -(\alpha-\beta)=\alpha^\star-\beta^\star\end{cases} \iff \begin{cases}\alpha=\beta^\star \\ \beta=\alpha^\star\end{cases} \tag{31}$$

Equation (30) translates to $(g_{12},\, g_{13}) = (g_{12}^\star,\, g_{13}^\star)$, implying robot R1 satisfies its bearing tasks while (31) translates to the *flipped* formation shape with bearings satisfying $(g_{12},\, g_{13}) = (g_{13}^\star,\, g_{12}^\star)$. It follows the bearing error signals are $e_{12\mathrm{b}} = -e_{13\mathrm{b}} = -b_{\mathrm{diff}}^\star$. With both g_{12} and g_{13} defined, we obtain $d_{12} \neq 0$ and $d_{13} \neq 0$; hence $z_{12} = \mathbb{0}_2$ and $z_{13} = \mathbb{0}_2$ are both infeasible. Robots R2 and R3 will stop moving when $e_{12\mathrm{d}} = 0$ and $e_{13\mathrm{d}} = 0$ holds, i.e., when they accomplished their individual distance task irrespective of R1. ■

It can be verified that the signed area of the flipped formation satisfies $S_{\mathrm{A_F}} = -S_{\mathrm{A}}^\star$.

B. Moving configurations

Proposition 4 ((**1B2D**) *Moving Configurations):* The moving configurations occur when the robots are co-linear, i.e., $g_{12} = \pm g_{13}$ and oriented in the direction of $b_{\mathrm{sum}}^\star = g_{12}^\star + g_{13}^\star$.

Proof: Expanding (28) yields

$$\begin{aligned}\left(K_{\mathrm{d}} e_{12\mathrm{d}} d_{12} + K_{\mathrm{b}}\right) g_{12} + K_{\mathrm{b}} g_{13} &= K_{\mathrm{b}} b_{\mathrm{sum}}^\star \\ K_{\mathrm{b}} g_{12} + \left(K_{\mathrm{d}} e_{13\mathrm{d}} d_{13} + K_{\mathrm{b}}\right) g_{13} &= K_{\mathrm{b}} b_{\mathrm{sum}}^\star.\end{aligned} \tag{32}$$

Solving for $\dot{z}_{23} = \mathbb{0}_2$, we obtain $e_{12\mathrm{d}} d_{12} g_{12} = e_{13\mathrm{d}} d_{13} g_{13}$. Two vectors are equal when they have the same magnitude and direction or opposite signs in both the magnitude and direction. Hence we distinguish the cases $g_{12} = g_{13} \wedge e_{12\mathrm{d}} d_{12} = e_{13\mathrm{d}} d_{13}$ and $g_{12} = -g_{13} \wedge e_{12\mathrm{d}} d_{12} = -e_{13\mathrm{d}} d_{13}$. Since $g_{12} = \pm g_{13}$, we conclude the robots are co-linear. Substituting this in (32), we obtain expressions of the form $h\, g_{12} = K_{\mathrm{b}} d_{\mathrm{sum}}^\star g_{\mathrm{sum}}^\star$ where $h = K_{\mathrm{d}} e_{12\mathrm{d}} d_{12} + 2K_{\mathrm{b}}$ when $g_{12} = g_{13}$ and $h = K_{\mathrm{d}} e_{12\mathrm{d}} d_{12}$ when $g_{12} = -g_{13}$. From this, we infer $g_{12} = \pm g_{\mathrm{sum}}^\star$, implying the orientation of the formation is in the direction of $b_{\mathrm{sum}}^\star$. ■

In light of Proposition 4, we can obtain *four* different ordering of the robots, as depicted in Fig. 3. To provide a full characterization of the moving configurations, it remains to obtain the inter-robot distances for the different ordering. We first derive expressions for the distance error corresponding to the different ordering from the general expression $h\, g_{12} = K_{\mathrm{b}} d_{\mathrm{sum}}^\star g_{\mathrm{sum}}^\star$. Define $e_{12\mathrm{d}} = {}^{s}/_{d_{12}}\, R_{\mathrm{bd}}$ and $e_{13\mathrm{d}} = {}^{t}/_{d_{13}}\, R_{\mathrm{bd}}$. For the different robot orderings in Fig. 3, we have for s and t

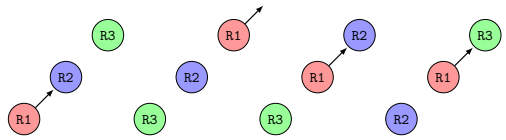

Fig. 3. Robot ordering for the moving configurations in the (**1B2D**) setup; the black arrow is the bearing vector $g_{\mathrm{sum}}^\star$. From left to right, we have ordering I to IV. Despite the different colors, both R2 and R3 are distance robots.

I. $g_{12} = g_{13} = g_{\mathrm{sum}}^\star$; $s = t = -2 + d_{\mathrm{sum}}^\star$;
II. $g_{12} = g_{13} = -g_{\mathrm{sum}}^\star$; $s = t = -2 - d_{\mathrm{sum}}^\star$;
III. $g_{12} = -g_{13} = g_{\mathrm{sum}}^\star$; $s = -t = d_{\mathrm{sum}}^\star$;
IV. $g_{12} = -g_{13} = -g_{\mathrm{sum}}^\star$; $s = -t = -d_{\mathrm{sum}}^\star$.

When expanded, we obtain the cubic expression in Lemma 1 with coefficients $c = -d_{12}^\star$ and $d = -s\, R_{\mathrm{bd}}$ when solving for feasible distance d_{12} while $c = -d_{13}^\star$ and $d = -t\, R_{\mathrm{bd}}$ when we are considering distance d_{13}. Since $d_{\mathrm{sum}}^\star \in \{0,\, 2\}$, it follows the value for s and t can be positive or negative and hence also the coefficient d of the cubic equation. In turn, this may impose a condition on the desired distances $d_{12}^\star$ and $d_{13}^\star$ for obtaining positive values for d_{12} and d_{13} as discussed in Section II-C. In particular, we can verify that coefficient d has range $d \in (-2,\, 4)\, R_{\mathrm{bd}}$. Taking $d = 4R_{\mathrm{bd}}$, we obtain that all four robot orderings in Fig. 3 can occur when the desired distances satisfy $d_{ij}^\star \geqslant \sqrt{3}\sqrt[3]{2R_{\mathrm{bd}}}$.

In the next part, we will show that the co-linear moving formations are unstable.

C. Local stability analysis of the equilibrium and moving formations

We have characterized the equilibrium configurations and the moving configurations. It is of interest to study the local stability property of these different sets. Similar to the stability analysis for the (**1D2B**) setup, we will use Lyapunov's indirect method. The Jacobian matrix corresponding to the z-dynamics (28) results in

$$A = -\begin{bmatrix} K_{\mathrm{b}} A_{12\mathrm{b}} + K_{\mathrm{d}} A_{12\mathrm{d}} & K_{\mathrm{b}} A_{13\mathrm{b}} \\ K_{\mathrm{b}} A_{12\mathrm{b}} & K_{\mathrm{b}} A_{13\mathrm{b}} + K_{\mathrm{d}} A_{13\mathrm{d}}\end{bmatrix}, \tag{33}$$

with $A_{ij\mathrm{d}}$ and $A_{ij\mathrm{b}}$ as defined earlier.

We first consider equilibrium configurations (29).

Lemma 3: The Jacobian matrix A_{E} at the equilibrium configurations in $\mathcal{S}_p^{\mathrm{C}} \cup \mathcal{S}_p^{\mathrm{F}}$ is Hurwitz.

Proof: For the correct and desired equilibrium configurations in $\mathcal{S}_p^{\mathrm{C}}$, the Jacobian matrix (33) evaluates to

$$A_{\mathrm{E}}^{\mathrm{C}} = -\begin{bmatrix} x^\star & 0 \\ 0 & p^\star\end{bmatrix} \otimes I_2 - \begin{bmatrix} m^\star\, g_{12}^\star g_{12}^{\star\top} & p^\star\, J g_{13}^\star (J g_{13}^\star)^\top \\ x^\star\, J g_{12}^\star (J g_{12}^\star)^\top & n^\star\, g_{13}^\star g_{13}^{\star\top}\end{bmatrix}, \tag{34}$$

where x, y, p, q, m, n and the bearing matrices are previously defined in (17) and (18). Also, for the flipped equilibrium configurations in $\mathcal{S}_p^{\mathrm{F}}$, we obtain

$$A_{\mathrm{E}}^{\mathrm{F}} = -\begin{bmatrix} x^\star & 0 \\ 0 & p^\star\end{bmatrix} \otimes I_2 - \begin{bmatrix} m^\star\, g_{13}^\star g_{13}^{\star\top} & p^\star\, J g_{12}^\star (J g_{12}^\star)^\top \\ x^\star\, J g_{13}^\star (J g_{13}^\star)^\top & n^\star\, g_{12}^\star g_{12}^{\star\top}\end{bmatrix}. \tag{35}$$

The characteristic polynomial $\chi_{\mathrm{E}}(\lambda)$ corresponding to the Jacobian matrices $A_{\mathrm{E}}^{\mathrm{C}}$ and $A_{\mathrm{E}}^{\mathrm{F}}$ is the same, namely

$$\begin{aligned}\chi_{\mathrm{E}}(\lambda) = (\lambda + q^\star)(\lambda + y^\star)\ldots \\ \left(\lambda^2 + (p^\star + x^\star)\lambda + p^\star x^\star \sin^2\theta^\star\right).\end{aligned} \tag{36}$$

This article has been accepted for publication in a future issue of this journal, but has not been fully edited. Content may change prior to final publication. Citation information: DOI 10.1109/TAC.2021.3115881, IEEE Transactions on Automatic Control

The roots of (36) are

$$\lambda_1 = -q^\star, \quad \lambda_2 = -y^\star,$$
$$\lambda_{3,\,4} = -1/2\,(p^\star + x^\star) \pm 1/2\sqrt{(p^\star + x^\star)^2 - 4p^\star x^\star \sin^2\theta^\star} \tag{37}$$

We can verify that $0 < 4p^\star x^\star \sin^2\theta^\star \leqslant (p^\star + x^\star)^2$. This implies all λs are real. Also, $-(p^\star + x^\star) + \sqrt{(p^\star + x^\star)^2 - 4p^\star x^\star \sin^2\theta^\star} < 0$ and hence we conclude that all roots are negative real. ∎

This leads to the following main result:

Theorem 2: Consider a team of three robots arranged in the (**1B2D**) setup with closed-loop dynamics given by (27). Given an initial configuration $p\,(0)$ that is close to the desired formation shape, then the robot trajectories asymptotically converge to a point $\widehat{p} \in \mathcal{S}_p^{\mathrm{C}}$.

Proof: Following Lemma 3, we obtain that link trajectories locally asymptotically converge to the desired relative positions $z^\star$ when they are initialized in the neighborhood of it. With $z_{ij}^\star = d_{ij}^\star\, g_{ij}^\star$, it follows the robots also converge to a point $\widehat{p} \in \mathcal{S}_p^{\mathrm{C}}$. ∎

Employing Lyapunov's indirect method to the moving co-linear formations yields the following statement.

Theorem 3: Let $p \in \mathbb{R}^6$ be a configuration yielding a co-linear formation as depicted in Fig. 3. Then p is unstable.

Proof: We first obtain the matrix A_{M} and the corresponding characteristic polynomial $\chi_{\mathrm{M}}\,(\lambda)$. With $e_{12\mathrm{d}} = {}^{s}/_{d_{12}}\,R_{\mathrm{bd}}$, $e_{13\mathrm{d}} = {}^{t}/_{d_{13}}\,R_{\mathrm{bd}}$ and bearing vectors $g_{12\mathrm{M}}$ and $g_{13\mathrm{M}}$ oriented to $g_{\mathrm{sum}}^\star$, A_{M} takes the form

$$A_{\mathrm{M}} = -\begin{bmatrix} (s+1)x & 0 \\ 0 & (t+1)p \end{bmatrix} \otimes I_2 - \begin{bmatrix} m\, g_{\mathrm{sum}}^\star g_{\mathrm{sum}}^{\star\,\top} & p\, Jg_{\mathrm{sum}}^\star (Jg_{\mathrm{sum}}^\star)^{\top} \\ x\, Jg_{\mathrm{sum}}^\star (Jg_{\mathrm{sum}}^\star)^{\top} & n\, g_{\mathrm{sum}}^\star g_{\mathrm{sum}}^{\star\,\top} \end{bmatrix}, \tag{38}$$

where the variables x, y, p, q, m, and n are defined in (17). The characteristic polynomial $\chi_{\mathrm{M}}\,(\lambda)$ is

$$\chi_{\mathrm{M}}\,(\lambda) = (\lambda + pt + q)\,(\lambda + xs + y)\left(\lambda^2 + \mathbb{B}\lambda + \mathbb{C}\right), \tag{39}$$

where the coefficients are $\mathbb{B} = (p\,(t+1) + x\,(s+1))$ and $\mathbb{C} = px\,((t+1)\,(s+1) - 1)$. We explore the nature of the roots, hereby focusing on the coefficients of the quadratic polynomial. For the different orderings, we obtain

I. $\mathbb{B}=(p+x)(-1+d_{\mathrm{sum}}^\star)$ and $\mathbb{C}=px\big((-1+d_{\mathrm{sum}}^\star)^2-1\big)<0$;
II. $\mathbb{B}=(p+x)(-1-d_{\mathrm{sum}}^\star)<0$ and $\mathbb{C}=px\big((-1-d_{\mathrm{sum}}^\star)^2-1\big)$;
III. $\mathbb{B}=(p+x)+(x-p)d_{\mathrm{sum}}^\star$ and $\mathbb{C}=-(d_{\mathrm{sum}}^\star)^2 px<0$;
IV. $\mathbb{B}=(p+x)-(x-p)d_{\mathrm{sum}}^\star$ and $\mathbb{C}=-(d_{\mathrm{sum}}^\star)^2 px<0$.

We infer that the quadratic polynomial in (39) contains at least a root with positive real part since for each ordering, either $\mathbb{B}$ or $\mathbb{C}$ is negative. This implies matrix A_{M} is not Hurwitz; therefore the co-linear formations are unstable. ∎

Remark 3: The bearing-only control law proposed in [17] can be obtained from the current control law by $P_{g_{ij}} e_{ij\mathrm{b}} = -P_{g_{ij}} g_{ij}^\star$. After following the steps as we have carried out for the gradient-based bearing control law, we infer that the closed-loop dynamics for the (**1D2B**) and the (**1B2D**) robot setups contain only equilibrium configurations and no moving configurations. The incorrect equilibrium configurations, in which either one or both of the bearing vectors are incorrect, are found to be unstable after linearization; the desired equilibrium is almost globally stable.

V. NUMERICAL EXAMPLE

We consider two triangular formation shapes with the same distances $d_{12}^\star$ and $d_{13}^\star$ but different value for the internal angle $\theta^\star$ (Note: $\theta^\star = \cos^{-1}\left(g_{12}^{\star\top} g_{13}^\star\right)$). In particular, shape $\mathbf{T_1}$ has bearing vectors such that the internal angle is $\theta_{\mathbf{T_1}}^\star = 15^\circ$ while for shape $\mathbf{T_2}$, we take $\theta_{\mathbf{T_2}}^\star = 45^\circ$. We set the gain ratio R_{bd} to a value 4. Taking the different setups into consideration, the threshold distance such that moving formations (stable or unstable) exist is $\widehat{d} = 2\sqrt{3} \approx 3.4641$. We set the desired distances to $d_{12}^\star = d_{13}^\star = 4$ and assume $\angle g_{12}^\star = 0^\circ$. Thus, shape $\mathbf{T_1}$ and $\mathbf{T_2}$ has the following desired constraints:

$$\begin{aligned} \mathbf{T_1}&: d_{12}^\star = d_{13}^\star = 4;\ \angle g_{12}^\star = 0^\circ,\ \angle g_{13}^\star = 15^\circ; \\ \mathbf{T_2}&: d_{12}^\star = d_{13}^\star = 4;\ \angle g_{12}^\star = 0^\circ,\ \angle g_{13}^\star = 45^\circ. \end{aligned} \tag{40}$$

For shape $\mathbf{T_1}$, the moving formation for the (**1D2B**) setup is unstable, since $\cos^2(15^\circ) = 0.9330 > 0.9321$. Hence the constraint in (24) is violated. For shape $\mathbf{T_2}$, we obtain $\cos^2(15^\circ) = 0.5 < 0.9321$ satisfying constraint (24).

In the current example, we intentionally set first the gain ratio R_{bd} and then obtain desired distances $d_{ij}^\star$s in order to show the existence and local asymptotic stability of moving formations in the (**1D2B**) setup.

A. (**1D2B**) *Simulation Results*

For the three robots in the (**1D2B**) setup, we focus on the formation shape $\mathbf{T_2}$. The Jacobian matrix A_{M} for the moving formation with distances $d_{12} = d_{13} \approx 3.8686$ is checked to be Hurwitz. Therefore, employing the closed-loop dynamics (5) can, depending on the initial configuration $p\,(0)$, lead to robot trajectories moving with a constant velocity. In Fig. 4(b), we show such an outcome for a specific $p\,(0)$. Fig. 4(a) depicts an initial $p\,(0)$ leading to convergence to the correct shape.

B. (**1B2D**) *Simulation Results*

For the three robots in the (**1B2D**) setup, we focus on the formation shape $\mathbf{T_1}$. There are two equilibrium formations, namely the correct and desired formation and the flipped formation satisfying only the distance constraints but not the bearing constraints. Fig. 5(a) depicts an initial configuration $p\,(0)$ which converges to this flipped formation. Notice that the signed area corresponding to $p\,(0)$ is positive (counter-clockwise cyclic ordering of the robots) while the flipped formation has a negative signed area (clockwise cyclic ordering of the robots). Fig. 5(b) depicts an initial co-linear configuration $p\,(0)$ leading to the robots to move with a constant velocity when employing the closed-loop dynamics (27). When perturbed, it will converge either to the correct or the flipped formation shape.

VI. CONCLUSIONS & FUTURE WORK

In the current work, we have considered the formation shape problem for teams of three robots partitioned into two categories, namely distance and bearing robots. Our aim is to employ gradient-based control laws in a heterogeneous setting and provide a systematic study on the stability of the possible formation shapes that arise as a result. We have shown

This article has been accepted for publication in a future issue of this journal, but has not been fully edited. Content may change prior to final publication. Citation information: DOI 10.1109/TAC.2021.3115881, IEEE Transactions on Automatic Control

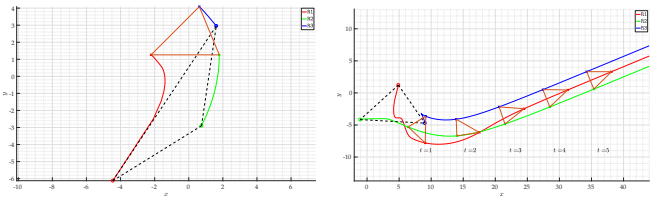

(a) Correct Formation (b) Moving Formation

Fig. 4. Robot trajectories for the (**1D2B**) setup; (, ,) = (R1, R2, R3), ∘ represents the initial and × is the final position. On the left panel, we have an initial configuration (dashed lines) where robots converge to the correct formation shape (solid lines) while the right panel illustrates an instance of convergence to the moving configuration with velocity $w = K_{\mathrm{b}} b^{\star}_{\mathrm{sum}}$.

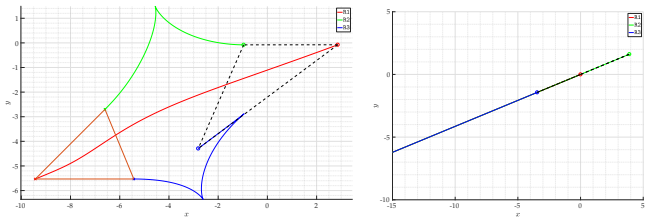

(a) Flipped Formation (b) Moving Formation

Fig. 5. Robot trajectories for the (**1B2D**) setup; On the left panel, we have an initial configuration where robots move and converge to the flipped formation shape while the right panel illustrates the evolution of the robots when the initial configuration satisfy conditions for ordering III in Fig. 3.

that under certain conditions on the distance and bearing error signals, we obtain distorted formation shapes moving with a constant velocity w. For the (**1B2D**) robot setup, these undesired formation shapes are unstable while for the (**1D2B**) robot setup, we derive conditions such that one of the distorted moving formation shape is locally asymptotically stable. When the gains K_{d} and K_{b} are chosen such that the required desired distances $d^{\star}_{ij}$s are smaller than a threshold distance $\hat{d}(K_{\mathrm{b}}, K_{\mathrm{d}})$, then moving formation shapes do not exist. Depending on the setup considered, this may lead to global asymptotic stability of the desired formation shape.

We note that the moving configurations in the (**1D2B**) setup and the flipped equilibrium configuration in the (**1B2D**) setup both have a signed area that has an opposite sign compared to the signed area of the desired formation shape. Hence the use of signed constraints as introduced in [15], [18] is a possible future direction. For the (**1D2B**) setup, the inclusion of the signed area constraint in [15] does not increase the sensing load of the distance robot while it can have the potential of mitigating the existence of distorted formation shapes.

REFERENCES

[1] W. Ren and R. W. Beard, *Distributed Consensus in Multi-vehicle Cooperative Control*. Springer, London, 2008.

[2] L. Krick, M. E. Broucke, and B. A. Francis, "Stabilisation of infinitesimally rigid formations of multi-robot networks," *International Journal of Control*, vol. 82, no. 3, pp. 423–439, Feb. 2009.

[3] F. Dörfler and B. A. Francis, "Formation control of autonomous robots based on cooperative behavior," in *2009 European Control Conference (ECC)*. IEEE, Aug. 2009, pp. 2432–2437.

[4] S. Zhao, Z. Li, and Z. Ding, "A Revisit to Gradient-Descent Bearing-Only Formation Control," in *2018 IEEE 14th International Conference on Control and Automation (ICCA)*. IEEE, Jun. 2018, pp. 710–715.

[5] L. Chen, M. Cao, and C. Li, "Angle rigidity and its usage to stabilize multi-agent formations in 2D," *IEEE Transactions on Automatic Control*, pp. 1–1, 2020.

[6] H. G. de Marina, "Maneuvering and robustness issues in undirected displacement-consensus-based formation control," *IEEE Transactions on Automatic Control*, 2020.

[7] S. Mou, M.-A. Belabbas, A. S. Morse, Z. Sun, and B. D. O. Anderson, "Undirected Rigid Formations Are Problematic," *IEEE Transactions on Automatic Control*, vol. 61, no. 10, pp. 2821–2836, Oct. 2016.

[8] S. Zhao and D. Zelazo, "Bearing Rigidity Theory and Its Applications for Control and Estimation of Network Systems: Life Beyond Distance Rigidity," *IEEE Control Systems Magazine*, vol. 39, no. 2, pp. 66–83, Apr. 2019.

[9] A. N. Bishop, M. Deghat, B. D. O. Anderson, and Y. Hong, "Distributed formation control with relaxed motion requirements," *International Journal of Robust and Nonlinear Control*, vol. 25, no. 17, pp. 3210–3230, Nov. 2015.

[10] Z. Sun, S. Mou, B. D. O. Anderson, and M. Cao, "Exponential stability for formation control systems with generalized controllers: A unified approach," *Systems & Control Letters*, vol. 93, pp. 50–57, Jul. 2016.

[11] N. P. K. Chan, B. Jayawardhana, and H. G. de Marina, "Stability analysis of gradient-based distributed formation control with heterogeneous sensing mechanism: Two and three robot case," *https://arxiv.org/abs/2010.10559*, 2020. [Online]. Available: https://arxiv.org/abs/2010.10559

[12] M.-A. Belabbas, S. Mou, A. S. Morse, and B. D. O. Anderson, "Robustness issues with undirected formations," in *2012 51st IEEE Conference on Decision and Control (CDC)*. IEEE, Dec. 2012, pp. 1445–1450.

[13] Z. Sun, M.-C. Park, B. D. O. Anderson, and H.-S. Ahn, "Distributed stabilization control of rigid formations with prescribed orientation," *Automatica*, vol. 78, pp. 250–257, Apr. 2017.

[14] H. G. de Marina, B. Jayawardhana, and M. Cao, "Distributed Rotational and Translational Maneuvering of Rigid Formations and Their Applications," *IEEE Transactions on Robotics*, vol. 32, no. 3, pp. 684–696, Jun. 2016.

[15] B. D. O. Anderson, Z. Sun, T. Sugie, S.-I. Azuma, and K. Sakurama, "Formation shape control with distance and area constraints," *IFAC Journal of Systems and Control*, vol. 1, pp. 2–12, Sep. 2017.

[16] T. Liu, M. de Queiroz, P. Zhang, and M. Khaledyan, "Further results on the distance and area control of planar formations," *International Journal of Control*, pp. 1–17, May 2019.

[17] S. Zhao and D. Zelazo, "Bearing Rigidity and Almost Global Bearing-Only Formation Stabilization," *IEEE Transactions on Automatic Control*, vol. 61, no. 5, pp. 1255–1268, May 2016.

[18] S.-H. Kwon, Z. Sun, B. D. O. Anderson, and H.-S. Ahn, "Hybrid distance-angle rigidity theory with signed constraints and its applications to formation shape control," *https://arxiv.org/abs/1912.12952*, 2019. [Online]. Available: https://arxiv.org/abs/1912.12952